Deciphering the pathogenic mechanism of CoQ_{10}-deficient glomerulopathy and optimizing therapeutic effect of drugs

Yu, Seyoung

Department of Medical Science

Graduate School

Yonsei University

Deciphering the pathogenic mechanism of CoQ_{10}-deficient glomerulopathy and optimizing therapeutic effect of drugs

Advisor Gee, Heon Yung

A Dissertation Submitted
to the Department of Medical Science
and the Committee on Graduate School
of Yonsei University in Partial Fulfillment of the
Requirements for the Degree of
Doctor of Philosophy in Medical Science

Yu, Seyoung

June 2025

Deciphering the pathogenic mechanism of CoQ_{10}-deficient glomerulopathy and optimizing therapeutic effect of drugs

This Certifies that the Dissertation of Yu, Seyoung is Approved

Committee Chair	**Nam, Ki Taek**
Committee Member	**Gee, Heon Yung**
Committee Member	**Yang, Jaeseok**
Committee Member	**Park, Hyun Woo**
Committee Member	**Jung, Hosung**

Department of Medical Science
Graduate School
Yonsei University
June 2025

ACKNOWLEDGEMENTS

I would like to express my deepest gratitude to my advisor, Professor Heon Yung Gee, for his unwavering support, invaluable guidance, and continuous encouragement throughout the completion of this dissertation. I am also sincerely thankful to the chair of my dissertation committee, Professor Ki Taek Nam, and to the committee members, Professors Jaeseok Yang, Hyun Woo Park, and Hosung Jung, for their thoughtful insights and constructive feedback. I would like to extend my heartfelt thanks to Professor Jin-Il Lee, who inspired and supported me to pursue this doctoral journey in the first place.

Throughout this long academic journey, I have received immense help from many people.

My sincere appreciation goes to Dr. Hye-Youn Kim for her warm support, and to the senior lab members who graduated before me: Kyeong Jee Cho, Jun Suk Lee, Dr. Yo Jun Choi, Dr. John Hoon Lim, Dr. Jisoo Lim, Dr. Dong Yun Kim, Dr. Jongwook Oh, and Dr. Young Ik Koh. Thanks to all of them, I was able to stay grounded and keep moving forward even in uncertain times.

I also want to thank Sun Young Joo, whom I deeply cherish, and the bright spirits of our lab: Dr. Ji Won Hong, Jung Ah Kim, Soyeon Lee, Yu Jin Sub, and Dr. Soo Kyung Seo, for filling our lab with joy and warmth. Because of them, my lab life remains a genuinely happy memory.

I am grateful to Dr. Dong Ki Lee, Dr. Seung Hyun Jang, Jae Won Noh, and Kyung Seok Oh, who taught me so much through their example in our daily lab life. From them, I learned not only scientific skills but also the values of humility, responsibility, and thoughtful collaboration.

Special thanks to my lovely junior lab members: Se Jin Kim, Hyeong Ki Song, Woo Chul Shin, and Essay Iyosaphit Endrias, for their energy and positivity. They brought constant laughter and light to the lab and helped me get through many difficult moments.

My deepest appreciation goes to Dr. Friedhelm Hildebrandt, Dr. Ken Saida, Dr. Caroline Kolvenbach, Selina Hölzel, and Shirlee Shril, who showed me the true meaning of a happy and inspiring lab life.

To everyone who supported me along the way, thank you from the bottom of my heart. I will always wish you success and happiness in all that you pursue.

Lastly, I dedicate this dissertation to my husband, my parents, my brother, and my parents-in-law, who have supported me with endless love, patience, and encouragement.

TABLE OF CONTENTS

LIST OF FIGURES

ABSTRACT

Deciphering the pathogenic mechanism of CoQ_{10}-deficient glomerulopathy and optimizing therapeutic effect of drugs.

Steroid-resistant nephrotic syndrome (SRNS) is characterized by proteinuria and is commonly associated with focal segmental glomerulosclerosis (FSGS), which can result from mutations in genes involved in coenzyme Q_{10} (CoQ_{10}) biosynthesis, such as PDSS2, COQ2, COQ6, and ADCK4. CoQ_{10} is an essential component of the mitochondrial inner membrane, playing a crucial role in electron transport in oxidative phosphorylation (OXPHOS) and protection against oxidative stress. While CoQ_{10} supplementation provides partial therapeutic benefits, its efficacy is inconsistent and has limitations. Therefore, it is crucial to elucidate the pathogenesis of CoQ_{10}-deficient glomerulopathy and establish optimal treatment conditions. This study utilized CoQ_{10}-deficient cell and animal models (podocyte-specific *Adck4* knockout mice, $Adck4^{\triangle Podocyte}$) and kidney organoids to investigate the effects of CoQ_{10} deficiency. CoQ_{10} deficiency due to ADCK4 loss led to mitochondrial dysfunction, including a reduction in membrane potential ($\Delta\Psi m$), which was not observed in HK-2 cells, indicating a greater susceptibility of podocytes to CoQ_{10} deficiency. In addition, CoQ_{10}-deficient podocytes exhibited increased oxidative stress, further highlighting their vulnerability to mitochondrial impairment. ADCK4 directly interacts with COQ5 and plays a crucial role in stabilizing the COQ complex. Loss of ADCK4 resulted in a decrease in COQ complex protein levels and a mild reduction in OXPHOS complex III expression. Consistent with this, CoQ_{10}-deficient kidney organoids exhibited normal overall morphology but displayed mitochondrial abnormalities in podocytes, reinforcing the importance of CoQ_{10} in maintaining mitochondrial homeostasis during kidney development. Single-cell RNA sequencing of kidney organoids derived

from CoQ_{10}-deficient iPSC lines (PDSS2-, COQ2-, ADCK4-Knockout) revealed preserved cell-type composition but distinct transcriptomic alterations in podocytes. Gene set enrichment analysis identified downregulation of oxidative phosphorylation and upregulation of TGF-β signaling, epithelial-to-mesenchymal transition, and apoptosis pathways, indicating mitochondrial dysfunction and early injury responses in CoQ_{10}-deficient podocytes. Additionally, the therapeutic potential of 2,4-dihydroxybenzoic acid (2,4-diHB), 2-probucol and Aspirin were evaluated using mice model, with a focus on the timing of treatment. Consistent with a previous study, early treatment (at 3 months) with 2,4-diHB successfully preserved kidney function in $Adck4^{\triangle Podocyte}$ mice, whereas delayed treatment (at 5 months) was ineffective. Furthermore, Probucol and Aspirin did not show significant therapeutic effects, suggesting that disease progression limits treatment efficacy and that early intervention is essential. In conclusion, this study emphasizes the role of ADCK4 in maintaining CoQ_{10} homeostasis and podocyte integrity, demonstrating that CoQ_{10} deficiency leads to mitochondrial dysfunction and progressive glomerular damage. The establishment of a CoQ_{10}-deficient kidney organoid model offers a robust platform for investigating disease mechanisms and evaluating targeted therapeutic strategies. Notably, early intervention with 2,4-diHB effectively preserved renal function, whereas delayed treatment failed to prevent disease progression, highlighting the urgency of timely therapeutic intervention in CoQ_{10}-associated nephropathy.

Key words : nephrotic syndrome; coenzyme Q 10; PDSS2; COQ2; COQ6; ADCK4; primary coenzyme Q 10 deficiency; kidney organoids; single cell RNA-sequencing; podocyte

1. Introduction

Nephrotic syndrome (NS) is a kidney disease defined by proteinuria with resulting hypoalbuminemia, frequently causing edema and hyperlipidemia [1-6]. "Steroid-resistant" NS can be distinguished from "steroids-sensitive" based on the patient's response to standard steroid therapy [7]. SRNS with the histological correlate of focal segmental glomerulosclerosis (FSGS) invariably leads to end-stage renal failure. SRNS is the second most common cause of chronic kidney disease in childhood. Over the past years, 63 genes have been identified as causing monogenic form of SRNS in human with an onset under their 30 years [8]. Most variants implicated in SRNS are found in highly expressed in the glomerular podocytes [9-11], implicating podocytes as the primary site of injury in NS. Podocytes are highly specialized epithelial cells that cover the outside of the glomerular capillary. Podocytes have a cell body with numerous primary, secondary and tertiary extensions, called foot processes. Adjacent foot processes are interconnected by slit diaphragms to form the final barrier to filtration and protects from the leakage of proteins [12].

Interestingly, a group of mutations in genes involved in coenzyme Q_{10} (CoQ_{10}, ubiquinone) biosynthesis, such as prenyl diphosphate synthase subunit 2 (PDSS2), COQ2, COQ6 and ADCK4 (COQ8B), have also been associated with childhood-onset FSGS and SRNS [13-15]. CoQ_{10} is a component of the mitochondrial inner membrane and plays important roles in supporting electron transport of oxidative phosphorylation (OXPHOS), protection from oxidative stress [16,17]. Disruption of CoQ_{10} biosynthesis in podocytes supports the view that mitochondrial function is crucial for the maintenance and function of the glomerular filtration barrier [18] whereas the neighboring tubular epithelial cells are spared early in disease despite higher mitochondrial content [19]. While mitochondria dysfunction is a hallmark of chronic kidney disease, recent work has demonstrated that mitochondria are dispensable for podocyte function and survival [19,20].

The patients with ADCK4 mutations represented adolescence-onset nephrotic syndrome and often progressed to End-stage kidney disease (ESKD) in the second decade of life [14,21]. ADCK4-associated glomerulopathy can be partially treated by CoQ_{10} supplementation [14,21-23]. However, its therapeutic efficacy was variable and limited because of poor oral availability. Another reason of limited response to CoQ supplementation can be attributed to the progression of renal disease to an irreversible stage. In yeast models, it is shown that CoQ intermediate precursors such as vanillic acid and 3,4-diHB improved the biosynthesis of CoQ6 [22,24]. In additions, treatment with 2,4-

dihydroxybenzoic acid (2,4-diHB) prevents FSGS progression and renal fibrosis in podocyte-specific *Coq6* knockout mice [25]. This 2,4-diHB was used to bypass ring precursor and able to restore endogenous CoQ biosynthesis, which is mediated by Coq7 hydroxylase [26], which implies that deeper understanding of CoQ_{10} biosynthesis may provide effective novel drugs for CoQ_{10}-deficient disease.

In previous studies, podocyte-specific *Adck4* knockout mice (*Adck4*$^{\Delta Podocyte}$) developed albuminuria at 4 months and represented abnormal glomeruli with significant fibrosis, disturbed podocyte morphology with foot process effacement [27]. The glomerular phenotype of *Adck4*$^{\Delta Podocyte}$ mice recapitulated aspects of the pathology of FSGS in humans resulting from *ADCK4* mutations. However, the precise mechanism of glomerular injury due to CoQ_{10}-deficiency has not been clearly described. Although the effects of 2,4-diHB were limited to the preventive effect, the treatment with 2,4-diHB improved survival, and reduced sclerotic glomeruli and expression of fibrotic markers, and maintained renal function. However, it is not certain whether these CoQ_{10} precursors are still effective even when renal function begins to decline. This makes it difficult to apply these drugs for clinical uses because most patients have already been diagnosed after renal function began to fail. In order to medicate properly after diagnosis, it is important to investigate pathogenic mechanisms of CoQ_{10}-deflicient glomerulopathy and validate therapeutic effects of drugs using elaborate manipulations.

In line with these findings, cellular models of ADCK4 deficiency have demonstrated that CoQ_{10} depletion in cultured podocytes leads to impaired mitochondrial respiratory chain activity, particularly complex II-III, and increased susceptibility to metabolic stress such as arachidonic acid exposure [27]. Notably, these mitochondrial dysfunctions were partially rescued by treatment with 2,4-diHB. Transmission electron microscopy further revealed podocyte-specfic mitochondrial defects, including abnormal fission and disrupted cristae, which were not observed in ADCK4-deficient HK-2 cells (human proximal tubular cells). Moreover, the CoQ_{10}-deficient podocytes displayed reduced cellular area, exacerbated under stress, indicating cytoskeletal and structural alterations. These in vitro observations highlight the podocyte-specific vulnerability to CoQ_{10}-deficiency and provide insights relevant to designing effective treatment strategies beyond the preventive stage.

Based on these results, it was hypothesized that uncharacterized mechanisms underlie CoQ_{10}-deficient podocyte-specific defects and that CoQ_{10}-deficient glomerulopathy may have an optimal treatment regimen to maximize therapeutic efficacy. To elucidate the pathogenesis of CoQ_{10}-deficient glomerulopathy, in vitro CoQ_{10}-deficient podocytes and kidney organoid models were

employed to examine their impaired function. Additionally, the therapeutic effects were evaluated by adjusting the timing of drug administration in *Adck4*$^{\Delta Podocyte}$ mice.

2. Materials and Methods

2.1. Mice

The animal experimental protocols were reviewed and approved by Yonsei University College of Medicine (#2015-0179). Mice were housed under pathogen-free conditions with a light period from 8:00 am to 8:00 pm and had ad libitum access to water and irradiated rodent chow (catalog #0006972; LabDiet, St. Louis, MO). *Nphs2.Cre+* (stock #008205) were obtained from Jackson Laboratory. The *Nphs2.Cre+;Adck4*$^{loxP/loxP}$ mouse model on C57BL/6 genetic background used in this study was generated from targeted *Adck4*$^{tm1a(EUCOMM)Hmgu}$ (*Adck4*^{tm1a}) embryonic stem cells obtained from EUCOMM. ES cells were injected into the blastocysts of mice. Chimeric mice were bred with C57BL/6J mice to establish germline transmission. *Adck4*$^{+/loxP}$ mice were crossed with *Nphs2.Cre+* mice and double heterozygous mice were crossed to generate podocyte-specific *Nphs2.Cre+;Adck4*$^{loxP/loxP}$ knockout mice and littermate controls. Genotyping was performed by PCR using the following primers: #1, GGATAGGGGGCTGGAGAGATG; #2, GCCCGCCTCCCTGTATCTTAG; #3, TCGGAGAGGAAAGGACTGGAG; #4, CCCTTTCCCTTGAGTTCACAGC; and #5, TGGCCTCAAACTCATGAAAATACTCC. Mice were maintained in mixed sex and were randomly assigned to the different experimental groups. For mouse studies, experimental results were validated over multiple litters, across several generations of the mouse colony with n>3. Data collection of urine, whole blood, and plasma analysis data were blinded to genotype so that the operator did not know the genotype during performing the measurements.

2.2. Supplementation of drugs to the mice in drinking water

Mice received drug treatments via both drinking water and chow to ensure continuous administration. 2,4-diHB was administered at a concentration of 25 mM in drinking water, which was refreshed twice a week. 2-probucol was provided at a concentration of 1% (w/w) in chow, allowing for ad libitum consumption. Additionally, acetylsalicylic acid was administered in drinking

water at a concentration of 1 mM, with water changed twice a week. The treatment regimen began at 5 months of age and continued until 8 months of age. Control mice received standard chow and untreated drinking water. Food intake and body weight were monitored regularly to ensure consistent drug consumption.

2.3. Cell culture

Human podocytes were a kind gift from Moin Saleem, University of Bristol, Bristol, UK, and cultured as previously described.33 Human podocytes were cultured in RPMI 1640 supplemented with 10% FBS and 1% penicillin/streptomycin and 1% insulin transferrin selenium. Human proximal tubule cells (HK-2) were maintained in DMEM supplemented with 10% FBS and 1% penicillin/streptomycin.

2.4. Gene editing

To establish *ADCK4* knockout (KO) cells, Single guide RNAs (sgRNAs) targeting human ADCK4 (sgRNA1, GCTGCACAATCCGCTCGGCAT; sgRNA2, GTAAGGTCTGCACAATCCGCT; and sgRNA3, GACCTTATGTACAGTTCGAG) were cloned into BsmBI-digested lentiCRISPR v2 (plasmid #52961; Addgene). lentiCRISPR v2, pMD2.G, and psPAX2 were transfected into Lenti-X 298T cells (Clontech). Supernatants containing lentivirus were collected 48 hours after transfection and passed through a 0.2 μM filter. Cultured podocytes and HK-2 cells were transduced with lentivirus, selected, and maintained with 4 μg/ml puromycin.

To establish CoQ10-deficient iPSCs, Precision gRNA Synthesis Kit (Invitrogen, #A29377) and TrueCutTM Cas9 Protein v2 (Invitrogen, #A36496) were used. gRNAs targeting PDSS2, COQ2, COQ6 and ADCK4 were synthesized respectively according to the manufacturer's instruction.

Target		5'-Sequences-3'
PDSS2	gRNA1	GCAACATCGCTATGCAGGTG
	gRNA2	GCCACGTTATCTTGGAGCCT
COQ2	gRNA1	CTCGGATTGACGTCATTCCC
	gRNA2	AACCGCATGAGGCGCAAGTA
COQ6	gRNA1	TTGGACCTGCTTCGAGCAAC
	gRNA2	GGCCCTGATAATGTTTGATA

ADCK4	gRNA1	TGACCGCTCTCGAGAACGCA
	gRNA2	TCAGCCGCTTGGCCAACTTT

Mouse embryonic fibroblasts were seeded one day before transfection in gelatin-coated 60 mm plate at 70% confluency. gRNAs were synthesized as manufacturer's instructions (Invitrogen). The iPSC were dissociated into single cells using Accutase (Accutase #AT104). The gRNA (10μg) and Cas9(5μg) proteins were transfected to iPSCs by electroporation using Super electroporator NEPA 21 typeII (NEPA GENE). For each electroporation experiment, the cell pellet was resuspended in Opti-MEM medium to a final concentration of 5*104 cells per 100 μL. For the electroporation a NEPA electroporator was used with the following set up; poring pulse: 125(V), 5(ms), 50(ms), 10(D.rate) + (polarity); transfer pulse: 20(V), 50(ms), 59(ms), 40(D.ate)+/-(polarity). After the cells were electroporated, they were transferred to a 60mm plate with mTeSR1 medium and monitored for at least 8 days.

2.5. Histologic analysis

The kidney tissues were fixed in 4% paraformaldehyde, sectioned (5 μm thickness), and stained with hematoxylin and eosin following the standard protocols for histologic examination.

2.6. Immunoblotting

Cells were incubated with lysis buffer [150 mM NaCl, 1 mM EDTA, 50 mM Tris-HCl (pH 7.4), 1% NP-40, and complete proteinase inhibitors], sonicated, and centrifuged at 13,200 rpm for 15 min. The supernatant was collected, and its protein concentration was measured by using Bradford assay. Absorbance at 590 nm was measured by using the SpectraMax microplate reader. The protein was mixed with 5x LDS sample buffer (KOMA) and loaded into a 4–12% Glycine-Tris gel (KOMA). The separated protein was then transferred to a nitrocellulose membrane. The blot was blocked with 5% skim milk at room temperature for 1 hr. Primary antibodies were diluted in 5% skim milk and incubated for overnight at 4°C. After washing with TBST, membranes were incubated with secondary antibodies. Protein blots were visualized by using West pico chemiluminescent substrate or West femto maximum sensitivity substrate kit (Pierce). Immunoblotting was quantified by densitometry using ImageJ software (National Institutes of Health, Bethesda, MD, USA).

2.7. Maintenance of human induced pluripotent stem cells

IMR90, human iPSCs (hiPSC derived from healthy fibroblasts; passage 16) were maintained in mTeSR1 (STEMCELL, #85850) in 6-well tissue culture plates (Falcon, #353046) coated with 1% vol/vol LDEV-Free hESC-qualified Geltrex (Life Technologies, #A1413302) in a 37°C incubator with 5% CO2. hiPSCs were passaged using Dissociation Solution for ReLeSR (STEMCELL, #05872) at a 1:5 split ratio every 5 days according to the manufacturer's protocol. ASE-9209 was purchased from Applied StemCell.

2.8. Differentiation of human induced pluripotent stem cells

hiPSCs grown on Geltrex were washed once with PBS (Life Technologies, #10010-049) and dissociated into single cells with Accutase (STEMCELL Technologies, #07920). Cells were then plated at a density of 5 × 104 or 1 × 101 cells/cm2 onto 24-well tissue culture plates (TPP, #92024) coated with 1% Geltrex in mTeSTR1 supplemented with the ROCK inhibitor Y27632 (10 μM) (TOCRIS, #1254).After 72 hours, cells (50% confluent) were briefly washed in PBS and then cultured in basic differentiation medium consisting of Advanced RPMI 1640 (Life Technologies, #12633-020) and 1X L-GlutaMAX (Life Technologies, #35050-061) supplemented with CHIR99021 (8–10 μM) (TOCRIS, #4423) for 4 days to induce late primitive streak cells Noggin (5 ng/ml) was also used for hiPSC differentiation in addition to CHIR (8-10 μM). To induce posterior intermediate mesoderm, cells were then cultured in Advanced RPMI + 1X L-GlutaMAX + activin (10 ng/mL) (R&D, #338-AC-050) for 3 days. For induction of nephron progenitor cells, the media was then changed to Advanced RPMI + 1X L-GlutaMAX + FGF9 (10 ng/ml) (R&D, #273-F9–025/CF) for 7 days. CHIR (3 μM) was added to the media from day 9 to 11 of differentiation to induce renal vesicles. On day 14, cells were switched to the basic differentiation medium and cultured for an additional 7 to 14 days (total of 21 to 28 days). The medium was replaced every 2 or 3 days.

2.9. Ultrastructural analysis

The kidney tissues and cells were fixed in 2.5% glutaraldehyde, 1.25% paraformaldehyde, and 0.03% picric acid in 0.1 M sodium cacodylate buffer (pH 7.4) overnight at 4°C. They were then washed with 0.1 M phosphate buffer, postfixed with 1% osmium tetroxide dissolved in 0.1 M PBS

for 2 hours, dehydrated in ascending gradual series (50%–100%) of ethanol, and propylene oxide was used for infiltration. Samples were embedded using the Poly/Bed 812 Kit (Polysciences) according to manufacturer's instructions. After pure fresh resin embedding and polymerization in a 65°C oven (TD-700; DOSAKA, Kyoto, Japan) for 24 hours, sections of approximately 200–250 nm thickness were cut and stained with toluidine blue for light microscopy. Sections of 70 nm thickness were double stained with 6% uranyl acetate (22400; EMS) for 20 minutes and lead citrate (Fisher) for 10 minutes for contrast staining. The sections were cut using a Leica EM UC-7 with a diamond knife (Diatome) and transferred onto copper and nickel grids. All the sections were observed by transmission electron microscopy (TEM; JEM-1011, JEOL, and Zeiss 912) at an acceleration voltage of 80 kV.

2.10. Statistical analysis

Statistical analyses were conducted using PRISM 8.0 (GraphPad, San Diego, CA, USA). All graphed results are expressed as means ± S.E.M. Statistical comparisons were made using two-way analysis of variance (ANOVA) with Bonferroni's corrections for multiple comparisons. Statistical significance is indicated in the figures as n.s., non-significant ($P > 0.05$), *$P < 0.05$, **$P < 0.01$, and ***$P < 0.001$. All other analyses were conducted with at least three independent experiments or samples to minimise statistical errors.

3. Results

3.1 Molecular and cellular consequences of coenzyme Q_{10} deficiency in podocytes

To investigate the role of Coenzyme Q_{10} (CoQ_{10}) in podocytes, ADCK4 knockout (KO) cultured podocytes were generated, and, for comparison, ADCK4 KO HK-2 cells (human proximal tubular cells) were also established (Figure 1A). Given the previously observed reduction in CoQ_{10} levels in ADCK4-deficient podocytes, these cell lines were subsequently used for functional and morphological analyses. As CoQ_{10} is known as an essential electron transfer carrier in the mitochondrial respiratory chain, mitochondrial membrane potential ($\Delta\Psi m$) was assessed using JC-10 and TMRM staining to determine whether this CoQ_{10} deficiency impacts mitochondrial function. CoQ_{10}-deficiency is expected to disrupt mitochondrial bioenergetics. Consistent with this, ADCK4 KO podocytes showed a marked decrease in $\Delta\Psi m$, which was partially restored by 2,4-diHB treatment (Figure 2A, B). In contrast, ADCK4 KO HK-2 cells retained normal mitochondrial membrane potential, further supporting the notion of podocyte-specific mitochondrial vulnerability (Figure 2C, D).

To further examine mitochondrial function, reactive oxygen species (ROS) levels were evaluated in podocytes. Basal ROS production was nearly twice as high in *ADCK4* KO podocytes compared to controls (Figure 3A). Mitochondrial superoxide levels, measured using MitoSOX staining, were also significantly elevated in *ADCK4* KO cells (Figure 3B). Furthermore, ADCK4 KO podocytes showed heightened sensitivity to oxidative stress induced by hydrogen peroxide (H_2O_2), a general ROS-generating agent, and tert-butyl hydroperoxide (tBHP), a lipid peroxidation inducer, as well as to arachidonic acid (AA), indicating increased mitochondrial oxidative stress. Notably, 2,4-diHB treatment reduced mitochondrial superoxide levels in both control and *ADCK4* KO podocytes, suggesting a protective effect.

To determine whether ADCK4 regulates COQ complex expression, mRNA and protein levels of COQ subunits were analyzed in podocytes. RT-PCR analysis revealed no significant differences in COQ complex gene expression between control and *ADCK4* KO podocytes, indicating that ADCK4 deficiency does not affect transcription (Figure 4A). However, western blot analysis showed a significant reduction in COQ complex protein levels in *ADCK4* KO podocytes, suggesting that

ADCK4 is essential for COQ protein stability (Figure 4B). Enzymatic activity assays further confirmed a decline in COQ complex function in *ADCK4* KO podocytes (Figure 4C).

Since ADCK4 is required for COQ complex stability, its interaction with COQ5, a key enzyme in the CoQ biosynthetic pathway, was subsequently investigated. Western blot analysis revealed a significant reduction in COQ5 protein levels in *ADCK4* KO podocytes, which was rescued by wild-type ADCK4 reintroduction and 2,4-diHB treatment (Figure 5A, B). Immunoprecipitation (IP) assays confirmed a direct interaction between ADCK4 and COQ5, as FLAG-tagged ADCK4 co-precipitated with endogenous COQ5 (Figure 5C). Further analysis showed that truncated ADCK4 mutants partially rescued COQ5, whereas missense-mutant ADCK4 proteins restored COQ5 stability to levels comparable to wild-type ADCK4 (Figure 5D).

Given the role of CoQ_{10} in the mitochondrial respiratory chain, OXPHOS complex levels were subsequently in podocytes. Western blot analysis showed a mild but significant reduction in Complex III protein levels in *ADCK4* KO podocytes, while other OXPHOS complexes remained unaffected (Figure 6A, B). In addition, COQ and OXPHOS complex stability was assessed in glomeruli from $Adck4^{\Delta Podocyte}$ mice. Western blot analysis revealed a significant reduction in COQ complex protein levels, supporting the idea that ADCK4 is required for COQ complex stability (Figure 7A, B). OXPHOS complex analysis showed a mild reduction in Complex III protein levels, whereas other mitochondrial respiratory chain complexes remained unchanged (Figure 7C, D).

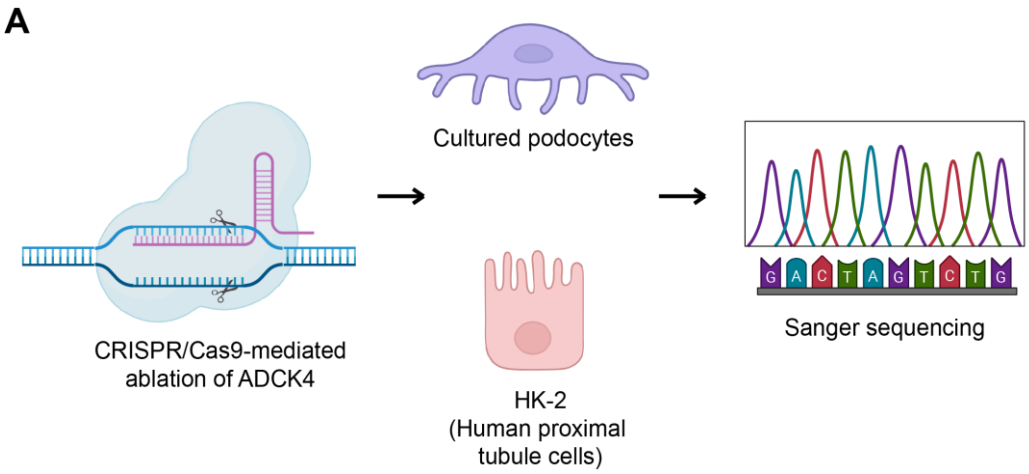

Figure 1. Schematic illustration of the generation and validation of ADCK4 knockout podocytes and HK-2 cells. (A) CRISPR-Cas9 genome editing was used to generate ADCK4 knockout in immortalized human podocytes and HK-2 cells. Successful gene disruption was confirmed by Saner sequencing.

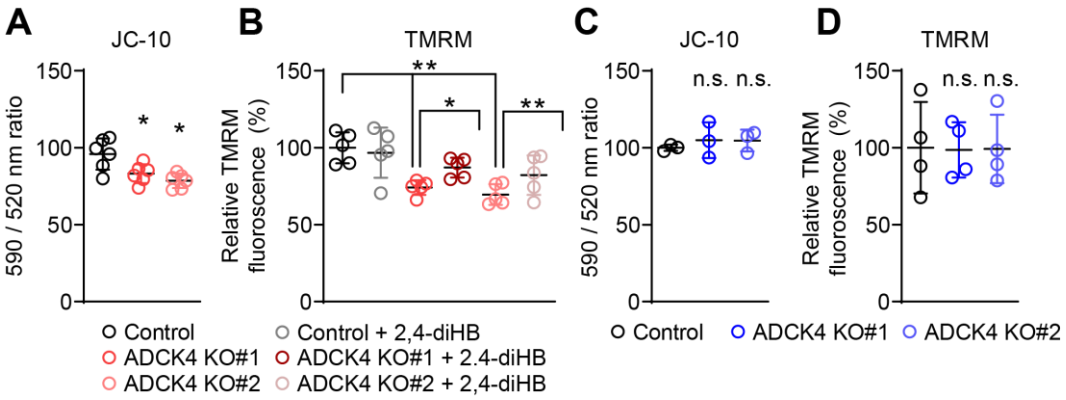

Figure 2. Coenzyme Q_{10} deficient-podocytes exhibit reduced mitochondrial membrane potential in podocytes but not in HK-2 cells. Podocytes (A-B) and HK-2 cells (C-D) were assessed for mitochondrial membrane potential (ΔΨ) using JC-10 and tetramethylrhodamine methyl ester (TMRM) staining. (A-B) *ADCK4* KO podocytes exhibited a decrease in ΔΨm compared to control podocytes. This reduction was partially restored with the addition of 500 mM 2,4-diHB. (C-D) *ADCK4* KO HK-2 cells showed normal ΔΨ compared to that of controls. Statistical analysis was performed using an unpaired t-test. *P < 0.05, **P < 0.005. Data are presented as mean ± SD.

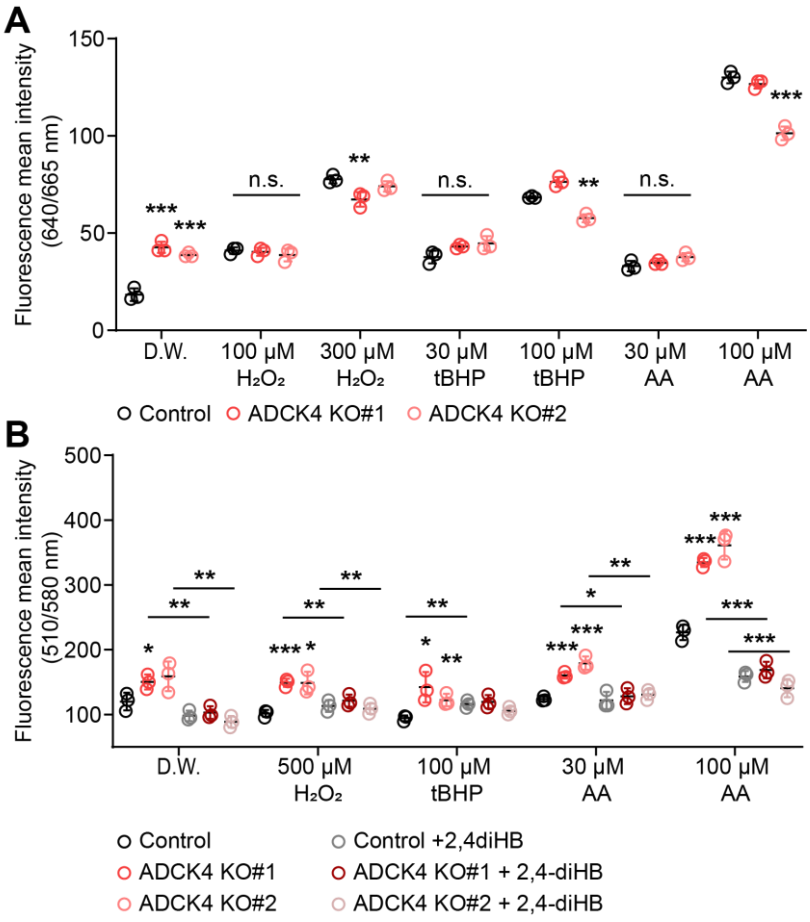

Figure 3. Coenzyme Q_{10} deficiency results in increased mitochondrial superoxide levels and altered ROS sensitivity in podocytes. (A) Cellular Reactive oxygen species (ROS) were measured using CellROX reagent. Basal ROS production was approximately twice as high in *ADCK4* KO cells compared to controls, exposure to H_2O_2, tBHP, or AA did not significantly alter ROS levels between the two groups. (B) Mitochondrial superoxide levels were measured using the MitoSOX reagent, revealing an increase in *ADCK4* KO cells. These cells demonstrated heightened sensitivity to oxidative stress induced by H_2O_2, tBHP, and particularly AA. Treatment with 2,4-diHB reduced mitochondrial superoxide levels in both control and *ADCK4* KO podocytes. Statistical analysis was performed using an unpaired t-test (*P < 0.05, **P < 0.005, ***P < 0.0001), with error bars representing mean ± SD. tBHP, tert-butyl hydroperoxide. AA, Arachidonic acid.

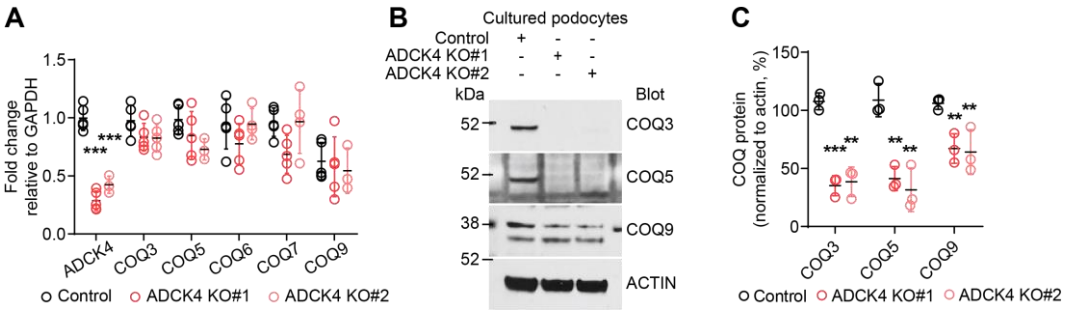

Figure 4. Loss of ADCK4 affects COQ complex protein stability but not mRNA levels in podocytes. (A) RT-PCR analysis of COQ complex gene expression in control and *ADCK4* KO podocytes. No significant differences in mRNA levels were observed between control and *ADCK4* KO cells, indicating that ADCK4 deficiency does not affect COQ complex transcription. (B) Western blot analysis of COQ complex proteins. *ADCK4* KO podocytes exhibit reduced protein levels of key COQ complex components, suggesting that ADCK4 is critical for maintaining COQ complex protein stability. (C) Quantification of COQ complex activity. Statistical analysis was performed using an unpaired t-test, with error bars representing mean ± SD.

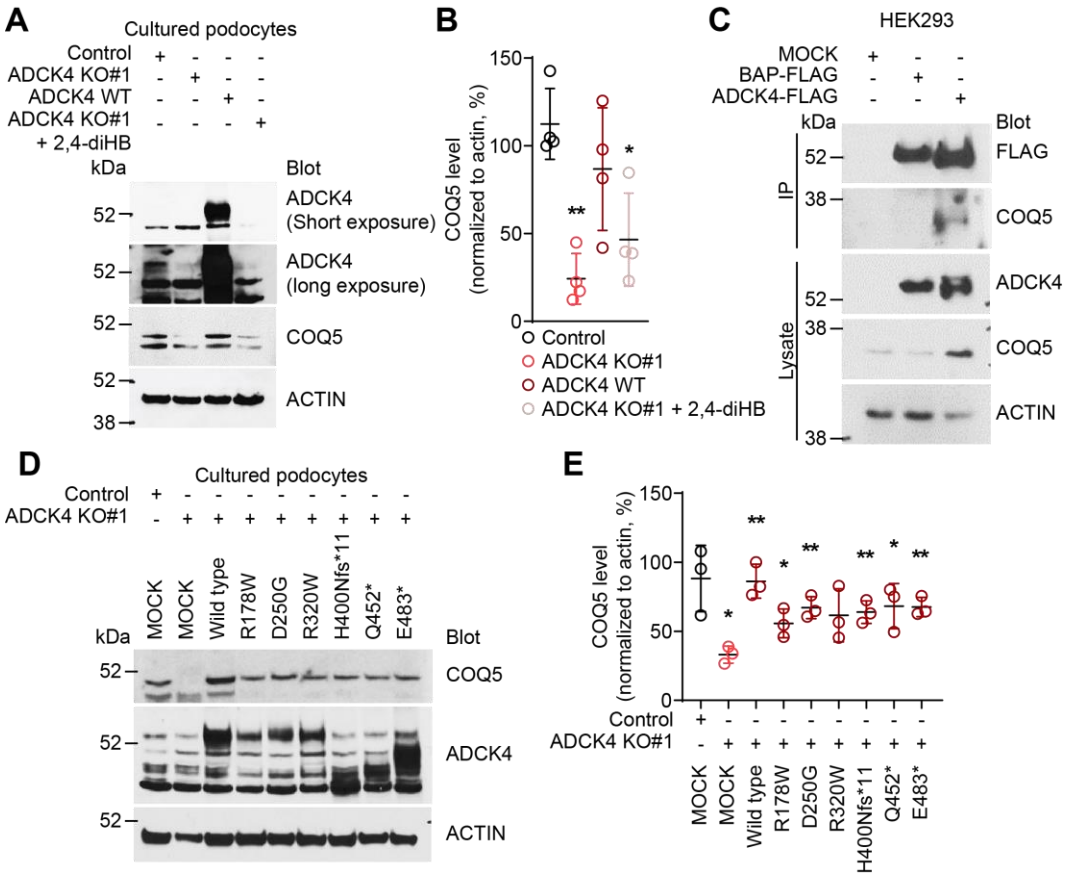

Figure 5. ADCK4 interacts with COQ5 and regulates its stability in podocytes. (A-B) Western blot analysis (A) and their quantification (B) shows a significant reduction in COQ5 protein expression in *ADCK4* KO podocytes compared to controls. Restoration of ADCK4 wild-type (WT) and 2,4-diHB treatment rescued COQ5 protein levels, suggesting that ADCK4 is critical for COQ5 stability. (C) Immunoprecipitation (IP) analysis confirming the interaction between ADCK4 and COQ5 in cultured podocytes. 3×FLAG-tagged ADCK4 or BAP was transfected into podocytes and immunoprecipitated using an anti-FLAG antibody, followed by immunoblot detection of endogenous COQ5. (D) Impact of ADCK4 mutations on COQ5 stabilization in ADCK4 KO podocytes. COQ5 levels were only partially rescued by truncated ADCK4 mutant proteins, whereas missense-mutated ADCK4 proteins restored COQ5 stability to levels comparable with wild-type ADCK4. (E) Statistical analysis was performed using an unpaired t-test, with error bars representing mean ± SD.

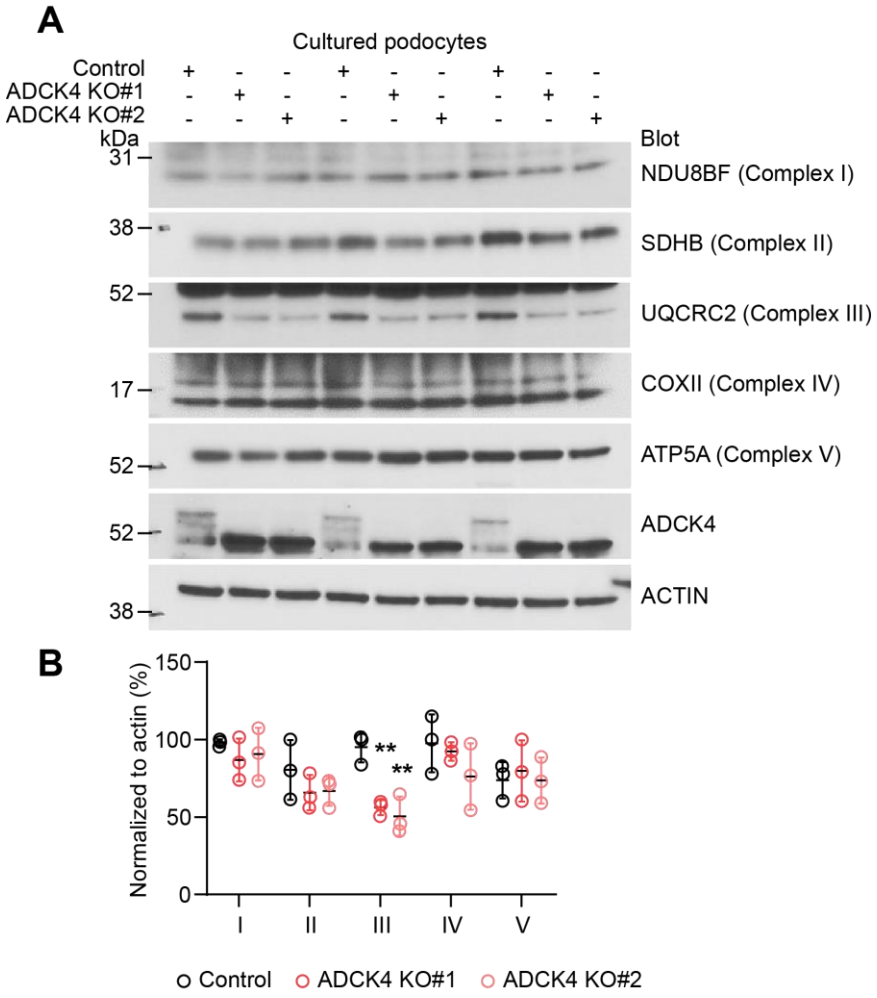

Figure 6. OXPHOS complex protein levels in *ADCK4* knockout podocytes. (A) Western blot analysis of mitochondrial oxidative phosphorylation (OXPHOS) complexes in control and *ADCK4* KO podocytes. Representative immunoblots show the expression levels of Complex I, Complex II, Complex III, Complex IV, and Complex V. (B) Quantification of OXPHOS complex protein expression. Densitometric analysis confirms a mild but significant reduction in Complex III levels in *ADCK4* KO podocytes compared to controls. Other OXPHOS complexes show no significant changes. Statistical analysis was performed using an unpaired t-test, with error bars representing mean ± SD.

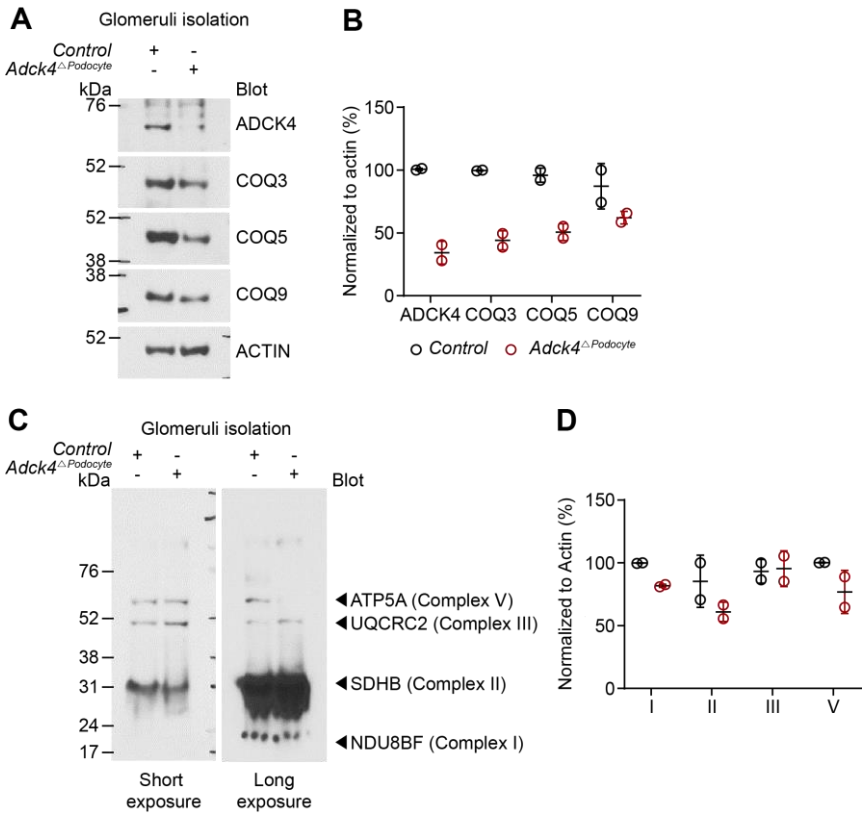

Figure 7. COQ complex and OXPHOS protein levels in Coenzyme Q_{10}-deficient mouse glomeruli. (A) Western blot analysis of the COQ complexes in *Adck4*$^{\triangle Podocyte}$ mouse glomeruli. Protein expression levels of key COQ complexes components were assessed in control and experimental groups. (B) Densitometric quantification confirms the reduction of COQ complexes in the absence of ADCK4, suggesting impaired stability or assembly. (C-D) Western blot analysis of the OXPHOS complex in *Adck4*$^{\triangle Podocyte}$ mouse glomeruli. Representative immunoblots (C) and densitometric quantification (D) reveal a mild reduction in Complex II protein levels, while other mitochondrial respiratory chain complexes remain largely unchanged. Statistical analysis was performed using an unpaired t-test, with error bars representing mean ± SD.

3.2 CoQ_{10}-deficiency induce mitochondrial alterations without disrupting kidney organoid morphogenesis

To investigate the role of CoQ_{10} in podocytes, *PDSS2*, *COQ2* and *ADCK4* KO induced pluripotent stem cells (iPSCs) were generated for each gene using CRISPR/Cas9-mediated gene editing. Sanger sequencing confirmed successful gene ablation, with *PDSS2* KO showing 75 bp and 171 bp deletions, *COQ2* KO exhibiting a 13 bp deletion, and *ADCK4* KO containing a 38 bp deletion. the generation of *COQ6* KO iPSCs was unsuccessful (Figure 8). Sequence chromatograms validated the specific regions of deletion, confirming the efficiency of the knockout strategy.

Kidney organoids were successfully differentiated from control and knockout iPSCs to assess their ability to self-organize into nephron-like structures. Bright-field microscopy revealed no overt morphological differences among control, *PDSS2*, *COQ2* and *ADCK4* KO organoids. Hematoxylin and eosin (H&E) staining demonstrated well-formed nephron-like structures in all conditions. Additionally, immunofluorescence staining for key nephron markers, including Lotus tetragonolobus lectin (LTL, green), nephrin (red), and E-cadherin (ECAD, white), confirmed proper segmentation and patterning of kidney organoids, suggesting that nephrogenesis remains unaffected in the absence of PDSS2, COQ2, or ADCK4 (Figure 9)

To assess whether podocyte differentiation and structural integrity were affected by the knockout of *PDSS2*, *COQ2* or *ADCK4*, immunofluorescence staining and transmission electron microscopy (TEM) were performed on kidney organoids. Nephrin (red) and WT1 (green) staining confirmed the presence of podocytes in all organoids, with no apparent differences in marker expression between control and knockout groups. Additionally, TEM analysis at 2900× and 6800× magnifications revealed normal podocyte foot process architecture and slit diaphragm structures across all conditions, indicating that podocyte ultrastructure remained unaffected despite genetic ablation of *PDSS2*, *COQ2*, or *ADCK4* (Figure 10).

Since PDSS2, COQ2 and ADCK4 play essential roles in coenzyme Q biosynthesis, mitochondrial morphology was examined in podocytes derived from control and knockout kidney organoids (Figure 11). TEM imaging revealed that podocytes from kidney organoids with deletions in each gene exhibited enlarged mitochondria, indicative of mitochondrial hypertrophy, compared to control podocytes. Additionally, quantification of mitochondrial number demonstrated a significant increase in *PDSS2* and *COQ2* KO podocytes, suggesting mitochondrial hyperplasia in response to gene ablation. Notably, *ADCK4* KO podocytes did not exhibit significant mitochondrial abnormalities

(Figure 11). These findings suggest that loss of PDSS2 and COQ2, but not ADCK4, leads to mitochondrial remodeling in podocytes, potentially disrupting energy homeostasis and cellular function.

To elucidate transcriptome-level changes induced by CoQ_{10} deficiency, single-cell RNA-seq was performed on day-21 kidney organoids derived from three CRISPR knock-out (KO) human iPSC lines (PDSS2-KO, COQ2-KO and ADCK4-KO) and an isogenic control (CTRL), allowing precise comparison of transcriptional profiles across all cell lineages. After quality filtering, 58,214 cells were jointly embedded with UMAP (Figure 12A). Unsupervised Leiden clustering (resolution = 0.4) identified 18 transcriptionally distinct populations that were annotated with canonical markers (Figure 12B). These included four podocyte clusters (Podocyte-1–4), proximal (PT) and distal (DT-1/2) tubular epithelia, nephron-progenitor cells (NPC-1/2), three mesenchymal clusters, endothelial, neuron-like and muscle-like cells, plus three minor “off-target” clusters.

Cell-type frequencies were largely comparable across genotypes, with no substantial shifts in the relative abundance of any lineage between control and CoQ_{10}-deficient organoids (Figure 15C). A violin plot of representative genes confirmed the robustness of the cell-type calls: NPHS2 and SYNPO were confined to podocytes, LRP2 and CUBN to PT cells, EPCAM broadly marked epithelia, and DCN highlighted stromal lineages (Figure 12D).

Podocytes were the primary cell type of interest; therefore, the podocytes were examined in greater detail. To achieve this, podocytes, and for comparison, proximal tubule (PT) were re-embedded and analyzed separately (Figure 13A-B). To look for disease-driven podocyte pathways, gene set enrichment analysis (GSEA) was applied on the podocyte cluster (Figure 13C). This analysis revealed Oxidative phosphorylation were significantly down-regulated in all three KO lines, consistent with impaired mitochondrial electron transport secondary to CoQ_{10} depletion. Conversely, TGF-β signaling, epithelial-to-mesenchymal transition and apoptosis gene sets were modestly enriched, hinting at maladaptive remodeling and early injury responses (Figure 13D).

These single-cell insights provide a mechanistic framework for understanding the early podocytopathy seen in CoQ_{10}-deficiency-associated nephrotic syndromes.

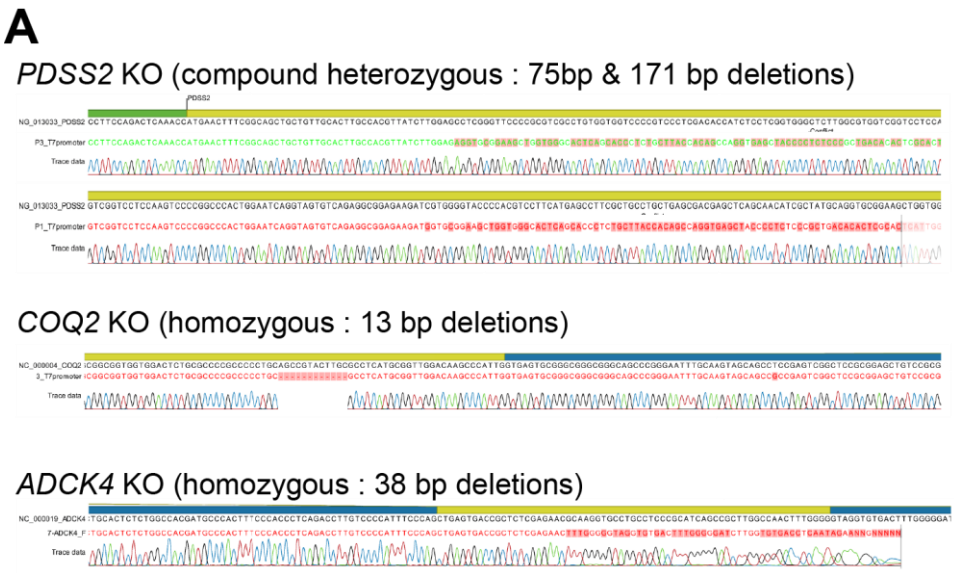

Figure 8. Sanger sequencing confirms the generation of *PDSS2*, *COQ2*, and *ADCK4* knockout iPSCs. (A) Sanger sequencing results validating the knockout of *PDSS2*, *COQ2*, and *ADCK4* in induced pluripotent stem cells (iPSCs). The *PDSS2* knockout (KO) exhibited deletions of 75 bp and 171 bp, while *COQ2* KO showed a 13 bp deletion. *ADCK4* KO displayed a 38 bp deletion. Sequence chromatograms indicate the deleted regions compared to reference sequences.

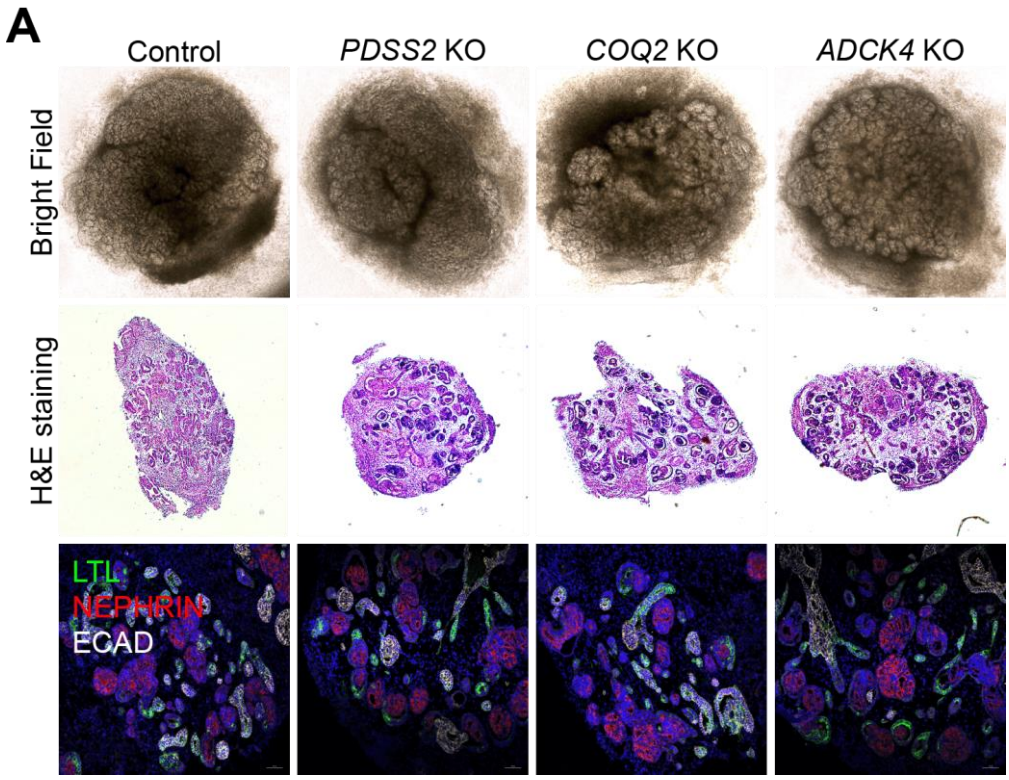

Figure 9. Kidney organoids from *PDSS*, *COQ2*, and *ADCK4* knockout iPSCs develop with intact structural organization. (A) Bright-field images, H&E staining, and immunofluorescence analysis of kidney organoids generated from control, *PDSS*, *COQ2*, and *ADCK4* KO iPSCs. Bright-field images show no significant morphological differences among the groups. H&E staining reveals well-formed nephron-like structures across all conditions. Immunofluorescence staining for lotus tetragonolobus lectin (LTL, green), nephrin (red), and E-cadherin (ECAD, white) indicates proper segmentation of nephron structures in all organoids.

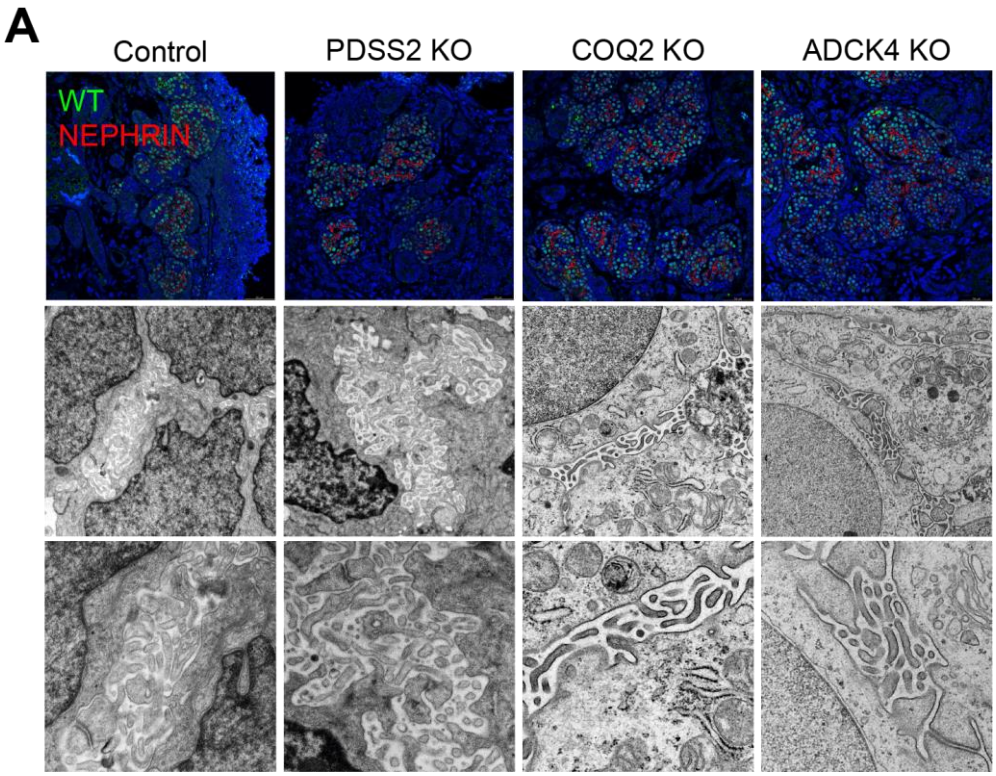

Figure 10. Podocyte architecture is preserved in PDSS2, COQ2, or ADCK4-deficient kidney organoids. (A) Immunofluorescence staining and transmission electron microscopy (TEM) images of podocytes in kidney organoids derived from control, *PDSS*, *COQ2*, and *ADCK4* KO iPSCs. Immunofluorescence staining for nephrin (red) and WT1 (green) indicates proper podocyte marker expression across all groups. TEM images at 2900× and 6800× magnifications reveal structurally intact podocyte foot processes, with no apparent ultrastructural abnormalities in knockout organoids compared to controls.

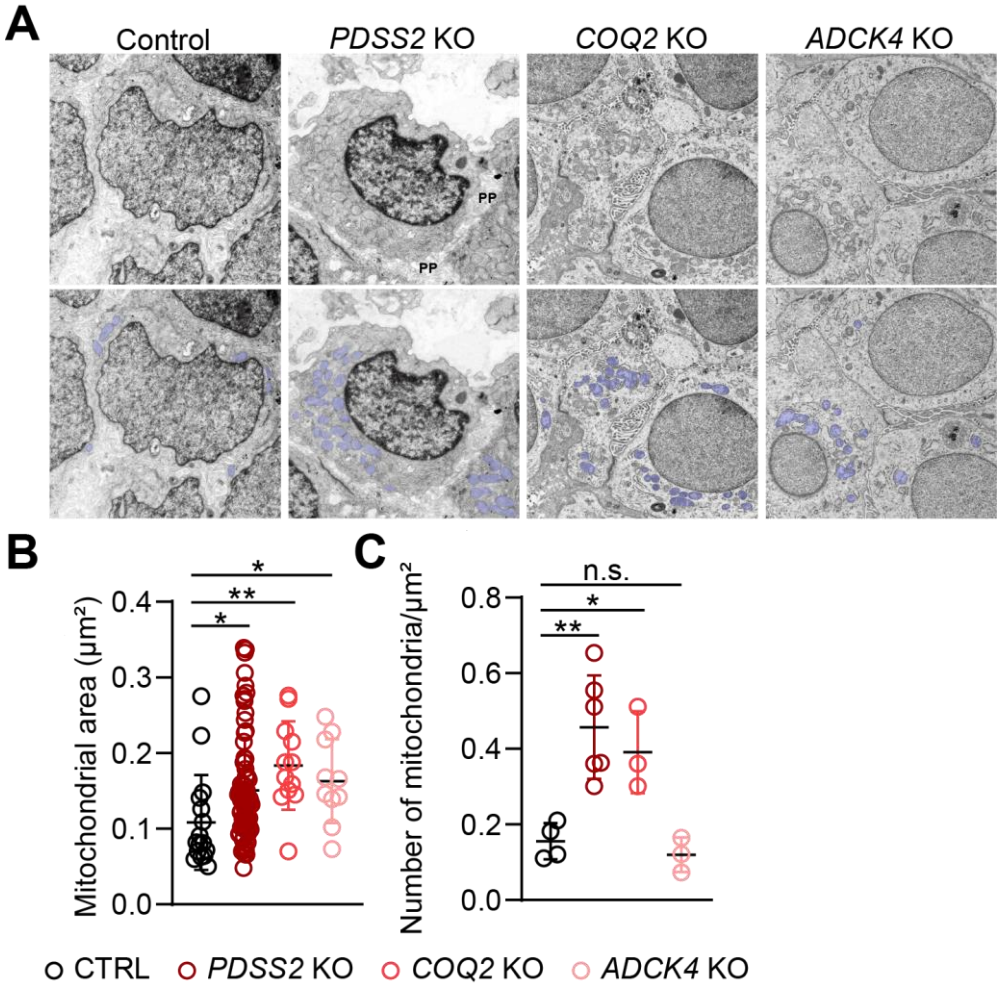

Figure 11. PDSS2 and COQ2 deficiency induces mitochondrial enlargement and hyperplasia in podocytes. (A) Transmission electron microscopy (TEM) images of podocytes from control, *PDSS*, *COQ2*, or *ADCK4* KO kidney organoids. Enlarged mitochondria are evident in *PDSS*, *COQ2*, or *ADCK4*-deficient podocytes compared to controls. (B) Quantification of mitochondrial number in podocytes. *PDSS2* and *COQ2* knockout podocytes demonstrate a significant increase in mitochondrial size, indicating mitochondrial hyperplasia. Statistical analysis was performed using an unpaired t-test, with error bars representing mean ± SD. PP, Primary process.

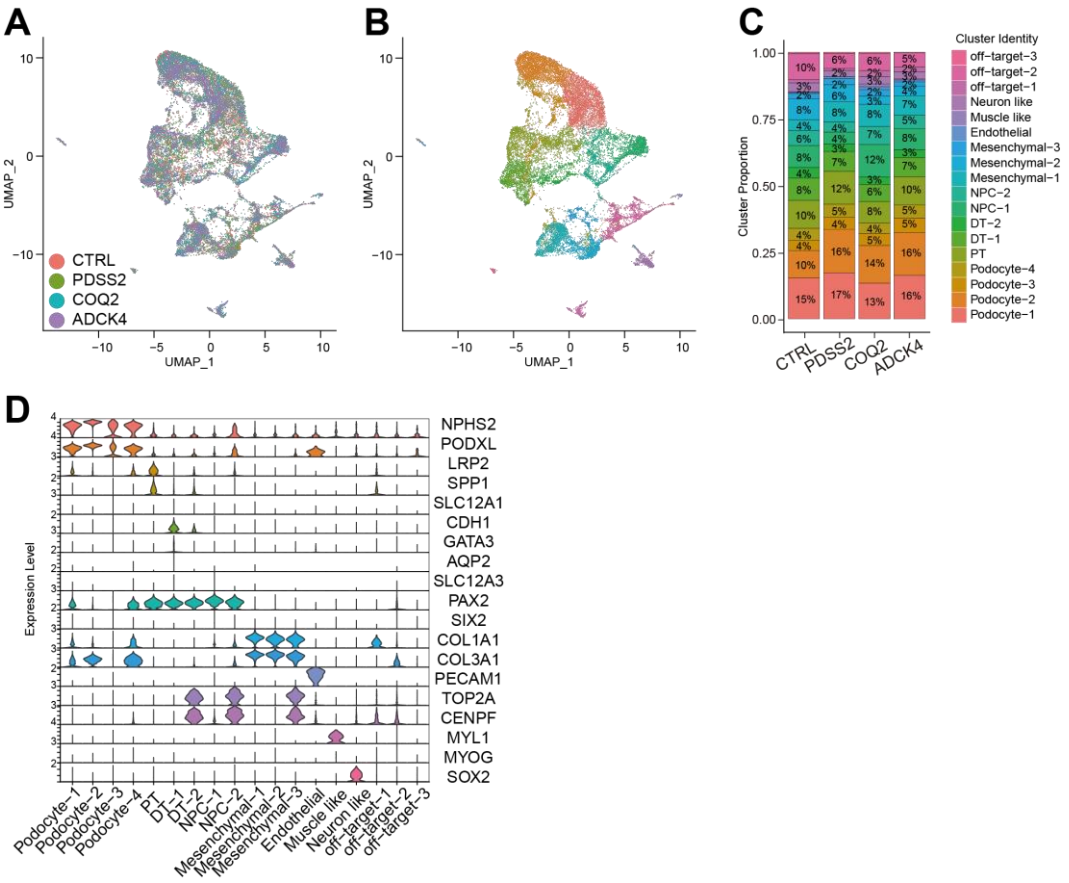

Figure 12. scRNA-seq analysis of the control and CoQ_{10}-deficient kidney organoids. (A) UMAP projection of the integrated single-cell transcriptomes from four conditions, Control (CTRL), PDSS2-KO, COQ2-KO and ADCK4-KO. (B) The same UMAP coloured by Leiden clusters (resolution 0.4). Eighteen transcriptionally distinct populations were annotated on the basis of canonical marker genes and are labelled Podocyte-1–4, Proximal Tubule (PT), Distal Tubule (DT-1/2), Nephron Progenitor Cell (NPC-1/2), Mesenchymal-1–3, Endothelial, Neuron-like, Muscle-like and three small "off-target" clusters. (C) Stacked bar plot comparing the proportion of each cluster across the four samples. (D) Violin plot of representative marker genes (columns) across clusters (rows) that supports the cell-type annotations in B.

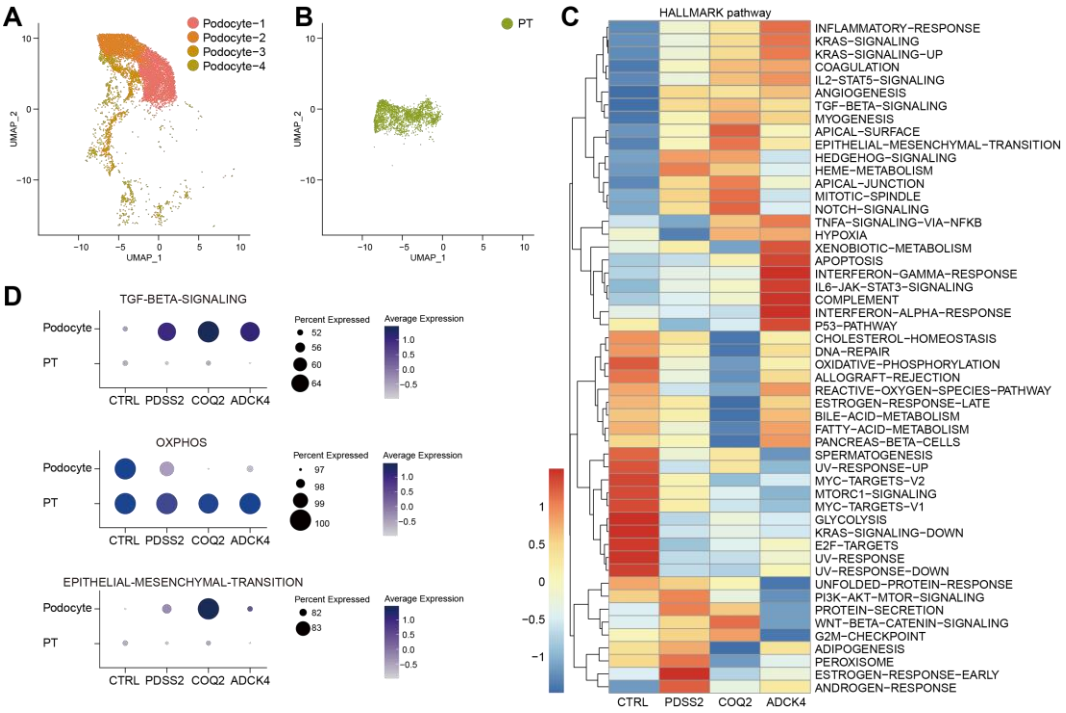

Figure 13. Podocyte-specific transcriptional re-wiring in CoQ_{10}-deficient organoids. (A-B) UMAP of the Podocyte or Proximal Tubule (PT) compartments. (C) Heatmap showing enrichment of hallmark genesets of the Molecular Signatures Database (MsigDB) in profiles of Podocytes from each sample. (D) Dot plot showing pathway enrichment scores across podocyte and PT clusters. Representative pathways related to TGF-β signaling, oxidative phosphorylation (OXPHOS), and epithelial–mesenchymal transition (EMT) are displayed. Circle size represents the proportion of cells expressing at least one isoform, while color indicates the mean expression level. Expression is markedly diminished in Podocytes from every knock-out line, whereas PT cells remain largely unaffected.

3.3 Delayed treatment leads to progressive kidney dysfunction and podocyte fibrosis

To evaluate the impact of early versus delayed treatment on kidney function, previously generated podocyte-specific *Adck4* knockout (*Adck4*$^{\Delta Podocyte}$) mice were employed (Figure 14A-B) [27]. Histological analysis revealed that early 2,4-diHB treatment preserved glomerular structure in *Adck4*$^{\Delta Podocyte}$ mice, whereas delayed treatment with 2,4-diHB, probucol, or aspirin did not prevent glomerular damage (Figure 15A). To assess kidney function, urinary albumin, blood urea nitrogen (BUN), and serum creatinine levels were measured following administration of 2,4-diHB, probucol, or aspirin at either 3 months (early) or 5 months (delayed). Mice treated early (3 months) with 2,4-diHB maintained normal kidney function, as indicated by stable urinary albumin, BUN, and serum creatinine levels (Figure 16A). However, mice receiving delayed treatment (5 months) exhibited a progressive decline in renal function, with significant increases in urinary albumin, BUN, and serum creatinine, regardless of whether they were treated with 2,4-diHB (Figure 16B), probucol (Figure 16C), or aspirin (Figure 16D). These findings indicate that once kidney dysfunction progresses beyond 5 months, therapeutic intervention is no longer effective in preserving renal function.

To further assess the structural consequences of delayed treatment, immunofluorescence staining for nephrin (podocyte marker) and α-smooth muscle actin (αSMA, fibrosis marker) was performed in glomeruli. Early treatment with 2,4-diHB preserved nephrin expression and suppressed αSMA upregulation, indicating that early-intervention maintained podocyte integrity and prevented fibrosis (Figure 17A). In contrast, delayed treatment with 2,4-diHB (Figure 17B), Probucol (Figure 17C), or Aspirin (Figure 17D) failed to restore nephrin expression or prevent fibrotic changes, as evidenced by increased αSMA staining. These results suggest that early intervention is critical for protecting podocytes and preventing fibrosis, while delayed treatment is ineffective in reversing established glomerular injury.

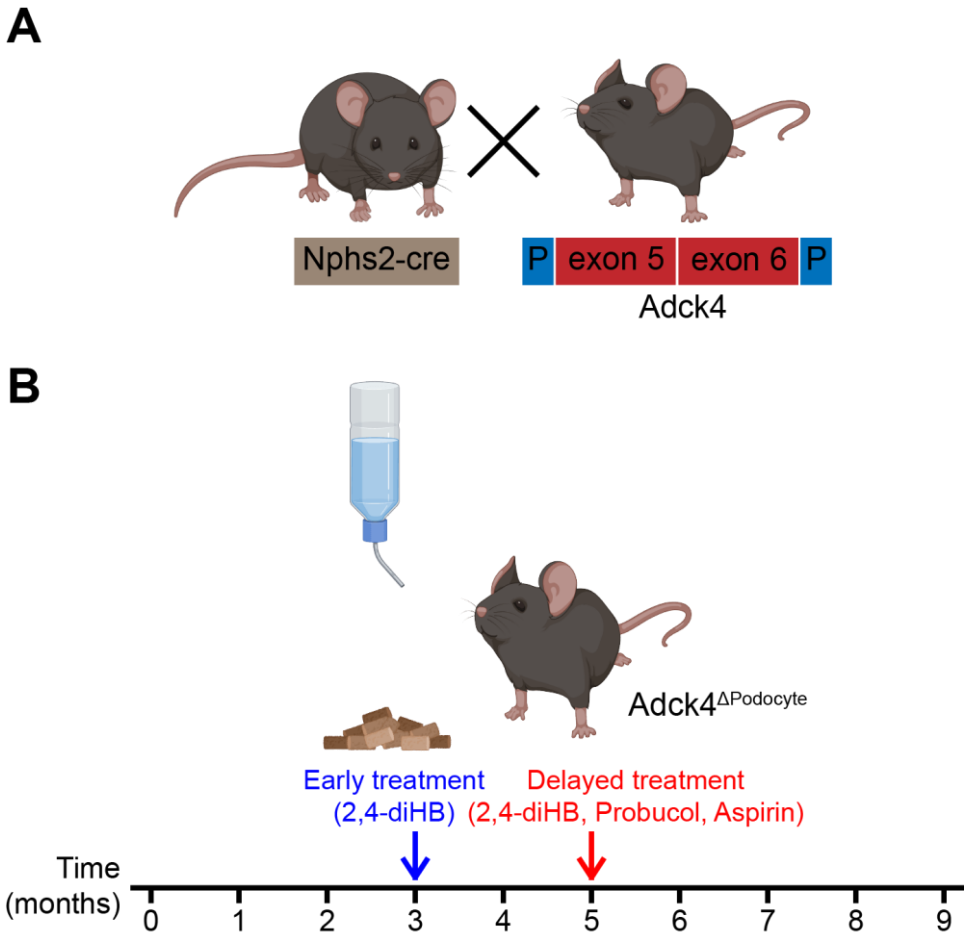

Figure 14. Schematic representation of early and delayed treatment in the *Adck4*$^{\Delta Podocyte}$ mouse model. (A) Podocyte-specific *Adck4* knockout (KO) mice, referred to as *Adck4*$^{\Delta Podocyte}$ were generated by crossing *Nphs2-Cre*$^{+}$ mice with *Adck4*$^{flox/flox}$ mice, in which exons 5 and 6 of the *Adck4* gene are flanked by loxP sites. (B) Mice were provided with treatment via drinking water or food, with two different intervention time points: early treatment (blue, 3 months) and delayed treatment (red, 5 months). This model was used to evaluate the therapeutic efficacy of 2,4-diHB, Probucol, and Aspirin in preserving kidney function in CoQ_{10} deficiency-associated nephropathy.

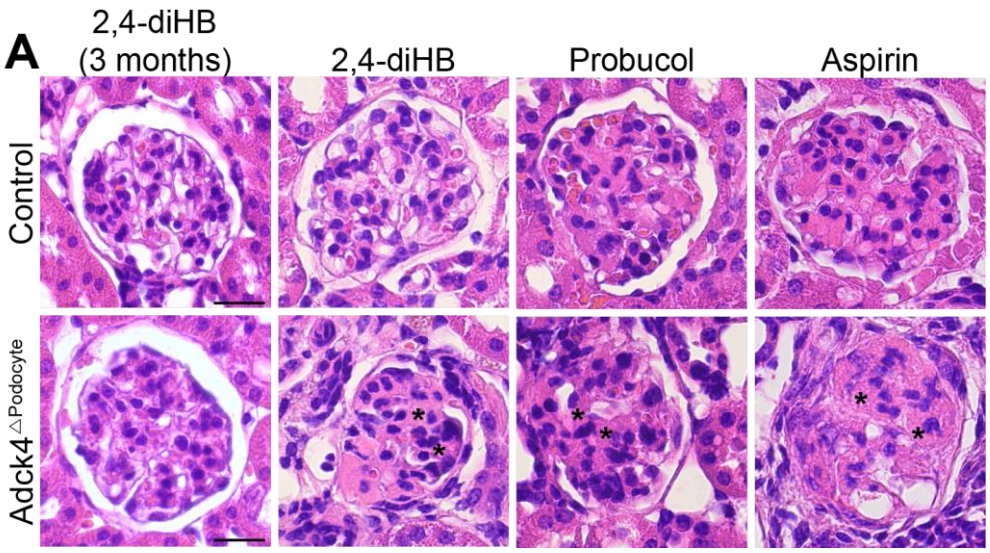

Figure 15. Early treatment with 2,4-diHB prevents renal pathology in podocyte-specific *Adck4* knockout mice, whereas delayed treatment is ineffective. (A) Hematoxylin and eosin (H&E) staining of glomeruli from control and *Adck4*$^{\triangle Podocyte}$ mice. *Adck4*$^{\triangle Podocyte}$ mice treated early (3 months) with 2,4-diHB (first column) exhibited preserved glomerular structure, indicating prevention of renal pathology. Delayed treatment (5 months) with 2,4-diHB, probucol, or aspirin failed to prevent glomerular damage, suggesting a lack of therapeutic efficacy at later stages.

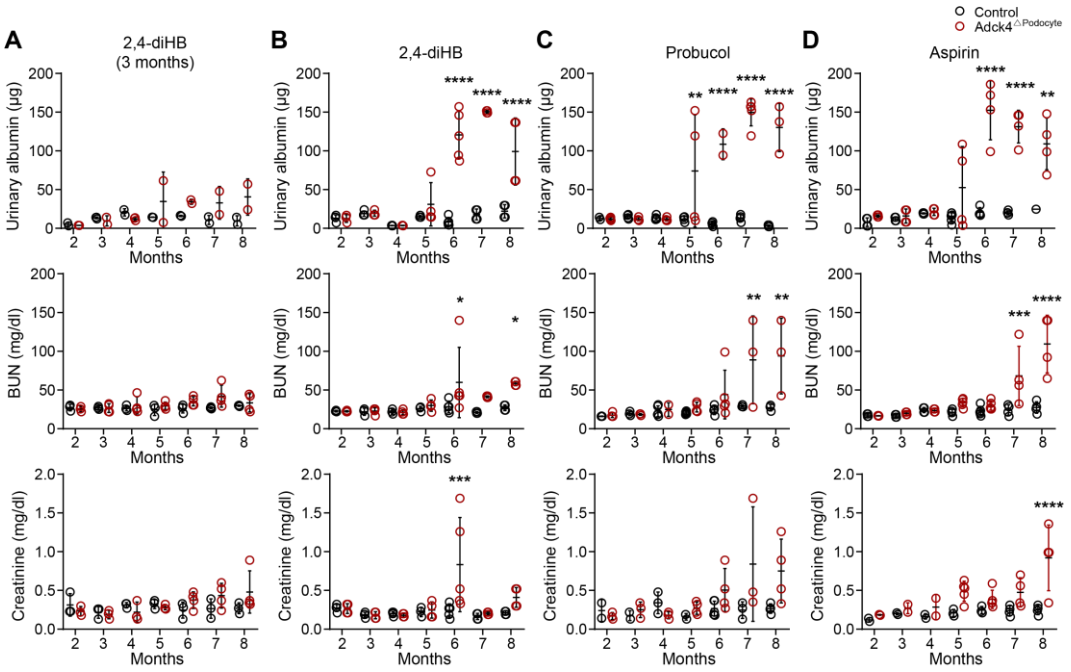

Figure 16. Delayed treatment leads to progressive decline in kidney function after 5 months. (A–D) Urinary albumin, blood urea nitrogen (BUN), and serum creatinine were measured to assess the kidney function in control and *Adck4*$^{\triangle Podocyte}$ mice following early (3 months) (A) or delayed (5 months) treatment with 2,4-diHB (B), probucol (C), or aspirin (D). Values and error bars are means ± S.E.M. *P < 0.05, **P < 0.01, ***P < 0.001, n.s. not significant, two-way ANOVA with Bonferroni's post hoc analysis.

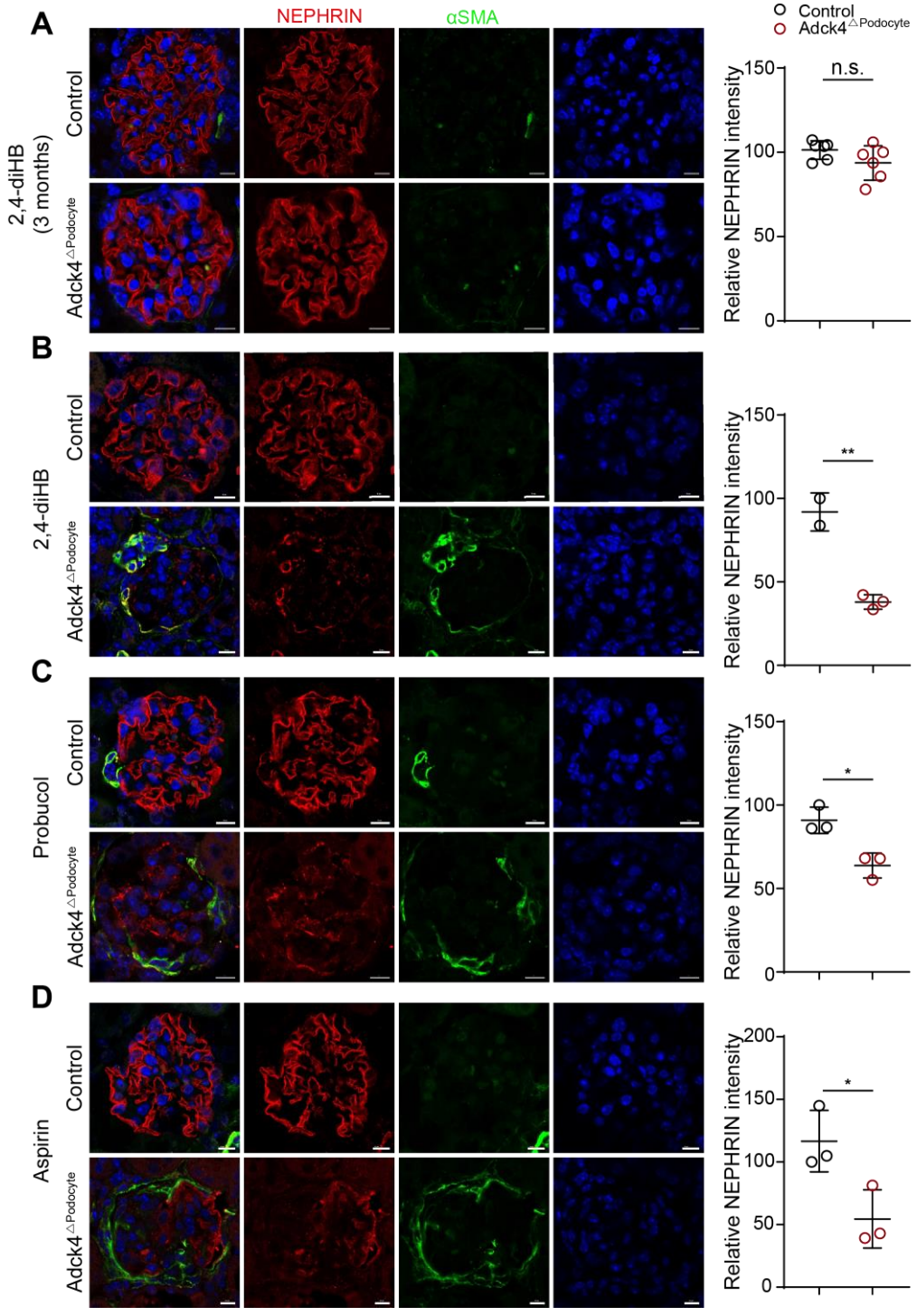

Figure 17. Early treatment with 2,4-diHB preserves podocyte integrity and prevents fibrosis, whereas delayed treatment is ineffective. (A–D) Immunofluorescence staining of podocyte marker nephrin (red) and fibrosis marker α-smooth muscle actin (αSMA, green) in glomeruli from control and *Adck4*$^{\triangle Podocyte}$ mice. DAPI (blue) stains nuclei. (A) Early treatment (3 months) with 2,4-diHB preserved nephrin expression and prevented αSMA upregulation, maintaining podocyte integrity and preventing fibrosis. (B–D) Delayed treatment (5 months) with 2,4-diHB (B), Probucol (C), or Aspirin (D) failed to restore nephrin expression or prevent fibrosis, as indicated by increased αSMA staining. Statistical analysis was performed using an unpaired t-test, with error bars representing mean ± SD.

4. Discussion

This study provides novel insights into the effects of CoQ_{10} deficiency on mitochondrial function, oxidative stress, podocyte integrity, and kidney pathology. CoQ_{10} deficiency was shown to disrupt mitochondrial homeostasis and cellular architecture in podocytes, based on analyses of genetically modified podocytes, kidney organoids, and a podocyte-specific *Adck4* knockout (*Adck4*$^{\triangle Podocyte}$) mouse model.

These findings reveal that loss of CoQ_{10} in podocytes leads to impaired mitochondrial function, characterized by reduced complex II-III activity, loss of mitochondrial membrane potential ($\Delta\Psi m$), and increased oxidative stress. These defects appear to be podocyte-specific, as HK-2 cells remained largely unaffected, highlighting the unique metabolic demands of podocytes and their heightened vulnerability to CoQ_{10} depletion. Notably, mitochondrial superoxide production was significantly elevated in CoQ_{10}-deficient podocytes, rendering them highly susceptible to oxidative stress. These findings align with previous studies demonstrating that podocytes rely heavily on mitochondrial metabolism and that oxidative damage contributes to glomerular disease progression in diabetic nephropathy [20,28-31].

Additionally, studies have shown that analogs of CoQ precursors bypass steps of CoQ biosynthesis and restore CoQ levels in yeast and mouse models [22,24,32]. These findings suggest that CoQ_{10} precursor analogs may serve as potential therapeutic agents for patients with CoQ_{10} deficiency-related renal dysfunction. Consistent with thie perspective, this study demonstrates that treatment with the CoQ precursor 2,4-diHB partially rescues mitochondrial function in ADCK4 KO

podocytes, further supporting its potential as a pharmacological intervention for CoQ_{10} deficiency-associated nephropathy.

CoQ_{10}-deficient podocytes also exhibit heightened susceptibility to mitochondrial damage, particularly in the presence of polyunsaturated fatty acids (PUFAs) such as arachidonic acid (AA). CoQ_{10}, in its reduced form (QH_2), acts as a potent lipid-soluble antioxidant, scavenging lipid peroxyl radicals and preventing oxidative damage to mitochondrial membranes. However, in CoQ_{10}-deficient conditions, this protective mechanism is impaired, leading to increased lipid peroxidation of PUFA-rich mitochondrial membranes. Arachidonic acid, due to its multiple double bonds, is highly prone to oxidative degradation. Without sufficient CoQ_{10}, this leads to mitochondrial membrane destabilization and impaired bioenergetics. Additionally, CoQ_{10} deficiency promotes electron leakage from the electron transport chain (ETC), leading to increased mitochondrial superoxide (O_2^-) production. The peroxidation of AA further amplifies reactive oxygen species (ROS) generation, creating a vicious cycle of oxidative damage that can compromises mitochondrial DNA integrity, protein stability, and cellular viability. Moreover, AA metabolism generates pro-inflammatory eicosanoids, which may exacerbate oxidative stress and inflammatory responses in podocytes. These findings suggest that oxidative stress, lipid peroxidation, and inflammation collectively contribute to the increased mitochondrial vulnerability observed in CoQ_{10}-deficient podocytes when exposed to AA.

Kidney organoids provide an isolated multicellular systems and enables the study of pathogenetic pathways, which is not feasible in classic monolayer podocytes cultures, as these lack interactions between different cell types and tissue organization [33]. The use of kidney organoids derived from CoQ_{10}-deficient iPSCs further confirmed that podocytes exhibit mitochondrial abnormalities despite the overall normal morphology of the organoids, reinforcing the essential role of CoQ_{10} in podocyte homeostasis.

For clinical application, determining the optimal timing of treatment is crucial, as therapeutic effects are most effective before renal dysfunction progresses to an irreversible stage. Additionally, the reduced form of CoQ (QH2) acts a potent antioxidant, scavenging free radicals and preventing lipid peroxidative damage. Based on this, it was hypothesized that CoQ_{10} deficiency-induced mitochondrial superoxide production triggers in cellular stress, which may be reversible through mitochondrial uncouplers such as salicylic acids [34,35]. While ADCK4-associated glomerulopathy can be partially managed with CoQ_{10} supplementation [27], its effectiveness is inconsistent. One possible

reason for treatment failure is the progression of renal disease to an irreversible stage, highlighting the need for early genetic diagnosis to identify ADCK4 mutations. Since ADCK4-associated glomerulopathy typically manifests around childhood often near the age of 10, timely diagnosis could allow for early intervention before the disease reaches a critical stage. Another contributing factor is CoQ_{10}'s poor oral bioavailability, which limits its therapeutic efficacy and leads to variability in patient outcomes. A key translational aspect of this study is the comparison between early (3 months) and delayed (5 months) treatment with 2,4-diHB, Probucol, and Aspirin in *Adck4* $^{\triangle Podocyte}$ mice. These results demonstrate that early intervention with 2,4-diHB successfully preserves kidney function and prevents glomerular damage, whereas delayed treatment fails to restore renal function.

This study highlights the critical role of CoQ_{10} in mitochondrial function, oxidative balance, and podocyte integrity. ADCK4 was shown to be essential for COQ complex stability, and early therapeutic intervention with 2,4-diHB was found to mitigate podocyte dysfunction. Furthermore, the use of CoQ_{10}-deficient kidney organoids provides a valuable platform for studying the molecular mechanisms of CoQ-associated nephropathy and identifying new therapeutic strategies. These findings reinforce the importance of timely intervention in CoQ_{10} deficiency-related kidney diseases and lay the foundation for future research into targeted therapies for mitochondrial dysfunction in glomerular disorders.

5. Conclusion

The mechanisms underlying podocyte dysfunction and potential therapeutic strategies for coenzyme Q_{10} (CoQ_{10}) deficiency remain incompletely understood. This study systematically examined the effects of CoQ_{10} depletion on mitochondrial function, oxidative stress, podocyte integrity, and kidney organoid development, providing new insights into the role of CoQ_{10} in maintaining mitochondrial and cellular homeostasis. The findings of this study demonstrate the following:

1 CoQ_{10} deficiency disrupts mitochondrial function in podocytes, leading to reduced mitochondrial complex II-III activity, abnormal cristae structure, and impaired mitochondrial membrane potential ($\Delta\Psi m$). These defects were podocyte-specific, as HK-2 cells remained unaffected.

2 ADCK4 plays a key role in stabilizing the COQ complex, particularly COQ5, without affecting COQ gene transcription. ADCK4 interacts directly with COQ5, and its loss leads to COQ protein instability and a mild reduction in OXPHOS complex III levels.

3 Kidney organoids derived from CoQ_{10}-deficient iPSCs develop normally in overall morphology but exhibit mitochondrial abnormalities in podocytes, reinforcing the essential role of CoQ_{10} in mitochondrial homeostasis during kidney development.

4 Early treatment (3 months) with 2,4-diHB effectively preserved kidney function and glomerular integrity in podocyte-specific *Adck4* knockout (*Adck4*$^{\Delta Podocyte}$) mice, whereas delayed treatment (5 months) with 2,4-diHB, Probucol, or Aspirin failed to restore renal function, emphasizing the importance of timely intervention.

Furthermore, this study may provide key information on the molecular consequences of CoQ_{10} deficiency in podocytes, the role of ADCK4 in COQ complex stability, and the importance of early therapeutic intervention in preserving kidney function. Additionally, the establishment of CoQ_{10}-deficient kidney organoids offers a valuable in vitro model to further investigate the mechanisms of CoQ_{10}-associated nephropathy and explore new therapeutic strategies.

REFERENCES

1. Lovric S, Ashraf S, Tan W, Hildebrandt F. Genetic testing in steroid-resistant nephrotic syndrome: when and how? Nephrology Dialysis Transplantation 2016;31:1802-13.
2. Vivante A, Hildebrandt F. Exploring the genetic basis of early-onset chronic kidney disease. Nat Rev Nephrol 2016;12:133-46.
3. Sadowski CE, Lovric S, Ashraf S, Pabst WL, Gee HY, Kohl S, et al. A single-gene cause in 29.5% of cases of steroid-resistant nephrotic syndrome. Journal of the American Society of Nephrology 2015;26:1279-89.
4. Landini S, Mazzinghi B, Becherucci F, Allinovi M, Provenzano A, Palazzo V, et al. Reverse phenotyping after whole-exome sequencing in steroid-resistant nephrotic syndrome. Clinical Journal of the American Society of Nephrology 2020;15:89-100.
5. Lovric S, Fang H, Vega-Warner V, Sadowski CE, Gee HY, Halbritter J, et al. Rapid detection of monogenic causes of childhood-onset steroid-resistant nephrotic syndrome. Clinical Journal of the American Society of Nephrology 2014;9:1109-16.
6. Tan W, Lovric S, Ashraf S, Rao J, Schapiro D, Airik M, et al. Analysis of 24 genes reveals a monogenic cause in 11.1% of cases with steroid-resistant nephrotic syndrome at a single center. Pediatric nephrology 2018;33:305-14.
7. Koide K, Sano M. Glucocorticoid therapy in renal diseases--its indication and therapeutic schedule. Nihon rinsho. Japanese Journal of Clinical Medicine 1994;52:728-33.
8. Klämbt V, Mao Y, Schneider R, Buerger F, Shamseldin H, Onuchic-Whitford AC, et al. Generation of monogenic candidate genes for human nephrotic syndrome using 3 independent approaches. Kidney international reports 2021;6:460-71.
9. Karaiskos N, Rahmatollahi M, Boltengagen A, Liu H, Hoehne M, Rinschen M, et al. A single-cell transcriptome atlas of the mouse glomerulus. Journal of the American Society of Nephrology 2018;29:2060-8.
10. Park J, Shrestha R, Qiu C, Kondo A, Huang S, Werth M, et al. Single-cell transcriptomics of the mouse kidney reveals potential cellular targets of kidney disease. Science 2018;360:758-63.
11. Qiu C, Huang S, Park J, Park Y, Ko Y-A, Seasock MJ, et al. Renal compartment–specific genetic variation analyses identify new pathways in chronic kidney disease. Nature

medicine 2018;24:1721-31.

12. Reiser J, Altintas MM. Podocytes. F1000Res 2016;5.
13. Mollet J, Giurgea I, Schlemmer D, Dallner G, Chretien D, Delahodde A, et al. Prenyldiphosphate synthase, subunit 1 (PDSS1) and OH-benzoate polyprenyltransferase (COQ2) mutations in ubiquinone deficiency and oxidative phosphorylation disorders. The Journal of clinical investigation 2007;117:765-72.
14. Ashraf S, Gee HY, Woerner S, Xie LX, Vega-Warner V, Lovric S, et al. ADCK4 mutations promote steroid-resistant nephrotic syndrome through CoQ 10 biosynthesis disruption. The Journal of clinical investigation 2013;123:5179-89.
15. Heeringa SF, Chernin G, Chaki M, Zhou W, Sloan AJ, Ji Z, et al. COQ6 mutations in human patients produce nephrotic syndrome with sensorineural deafness. The Journal of clinical investigation 2011;121:2013-24.
16. Ernster L, Dallner G. Biochemical, physiological and medical aspects of ubiquinone function. Biochimica et Biophysica Acta (BBA)-Molecular Basis of Disease 1995;1271:195-204.
17. Lenaz G, Genova ML. Mobility and function of coenzyme Q (ubiquinone) in the mitochondrial respiratory chain. Biochimica et Biophysica Acta (BBA)-Bioenergetics 2009;1787:563-73.
18. Müller-Deile J, Schiffer M. The podocyte power-plant disaster and its contribution to glomerulopathy. Frontiers in Endocrinology 2014;5:209.
19. Sidhom EH, Kim C, Kost-Alimova M, Ting MT, Keller K, Avila-Pacheco J, et al. Targeting a Braf/Mapk pathway rescues podocyte lipid peroxidation in CoQ-deficiency kidney disease. J Clin Invest 2021;131.
20. Brinkkoetter PT, Bork T, Salou S, Liang W, Mizi A, Özel C, et al. Anaerobic Glycolysis Maintains the Glomerular Filtration Barrier Independent of Mitochondrial Metabolism and Dynamics. Cell Rep 2019;27:1551-66.e5.
21. Korkmaz E, Lipska-Ziętkiewicz BS, Boyer O, Gribouval O, Fourrage C, Tabatabaei M, et al. ADCK4-associated glomerulopathy causes adolescence-onset FSGS. Journal of the American Society of Nephrology 2016;27:63-8.
22. Doimo M, Trevisson E, Airik R, Bergdoll M, Santos-Ocaña C, Hildebrandt F, et al. Effect of vanillic acid on COQ6 mutants identified in patients with coenzyme Q10 deficiency.

Biochimica et Biophysica Acta (BBA)-Molecular Basis of Disease 2014;1842:1-6.

23. Feng C, Wang Q, Wang J, Liu F, Shen H, Fu H, et al. Coenzyme Q10 supplementation therapy for 2 children with proteinuria renal disease and ADCK4 mutation: Case reports and literature review. Medicine 2017;96.
24. Ozeir M, Mühlenhoff U, Webert H, Lill R, Fontecave M, Pierrel F. Coenzyme Q biosynthesis: Coq6 is required for the C5-hydroxylation reaction and substrate analogs rescue Coq6 deficiency. Chemistry & biology 2011;18:1134-42.
25. Widmeier E, Airik M, Hugo H, Schapiro D, Wedel J, Ghosh CC, et al. Treatment with 2, 4-dihydroxybenzoic acid prevents FSGS progression and renal fibrosis in podocyte-specific Coq6 knockout mice. Journal of the American Society of Nephrology 2019;30:393-405.
26. Freyer C, Stranneheim H, Naess K, Mourier A, Felser A, Maffezzini C, et al. Rescue of primary ubiquinone deficiency due to a novel COQ7 defect using 2, 4–dihydroxybensoic acid. Journal of medical genetics 2015;52:779-83.
27. Widmeier E, Yu S, Nag A, Chung YW, Nakayama M, Fernández-del-Río L, et al. ADCK4 Deficiency Destabilizes the Coenzyme Q Complex, Which Is Rescued by 2,4-Dihydroxybenzoic Acid Treatment. Journal of the American Society of Nephrology 2020;31:1191-211.
28. Bhatti AB, Usman M. Drug targets for oxidative podocyte injury in diabetic nephropathy. Cureus 2015;7.
29. Chung SS, Ho EC, Lam KS, Chung SK. Contribution of polyol pathway to diabetes-induced oxidative stress. Journal of the American Society of Nephrology 2003;14:S233-S6.
30. Eid AA, Gorin Y, Fagg BM, Maalouf R, Barnes JL, Block K, et al. Mechanisms of podocyte injury in diabetes: role of cytochrome P450 and NADPH oxidases. Diabetes 2009;58:1201-11.
31. Lee HB, Yu M-R, Yang Y, Jiang Z, Ha H. Reactive oxygen species-regulated signaling pathways in diabetic nephropathy. Journal of the American Society of Nephrology 2003;14:S241-S5.
32. Xie LX, Ozeir M, Tang JY, Chen JY, Jaquinod S-K, Fontecave M, et al. Overexpression of the Coq8 kinase in Saccharomyces cerevisiae coq null mutants allows for accumulation of diagnostic intermediates of the coenzyme Q6 biosynthetic pathway. Journal of Biological Chemistry 2012;287:23571-81.

33. Romero-Guevara R, Ioannides A, Xinaris C. Kidney Organoids as Disease Models: Strengths, Weaknesses and Perspectives. Frontiers in Physiology 2020;11.
34. Zhao RZ, Jiang S, Zhang L, Yu ZB. Mitochondrial electron transport chain, ROS generation and uncoupling. International journal of molecular medicine 2019;44:3-15.
35. Norman C, Howell KA, Millar AH, Whelan JM, Day DA. Salicylic acid is an uncoupler and inhibitor of mitochondrial electron transport. Plant Physiol 2004;134:492-501.

Abstract in Korean

CoQ_{10} 결핍 사구체병증의 병리기전 규명과 약물 치료 효과의 최적화

스테로이드 저항성 신증후군(SRNS)은 단백뇨를 특징으로 하며, 흔히 국소분절성 사구체경화증(FSGS)과 관련되어 나타난다. 이 질환은 *PDSS2*, *COQ2*, *COQ6*, *ADCK4* 등 코엔자임 Q10(CoQ_{10}) 생합성과 관련된 유전자의 돌연변이로 인해 발생할 수 있다. CoQ_{10}은 미토콘드리아 내막의 필수 성분으로, 산화적 인산화(OXPHOS) 과정에서 전자 전달과 산화 스트레스 방어에 중요한 역할을 한다. CoQ_{10} 보충 요법은 부분적인 치료 효과를 보이기도 하지만, 효과가 일관되지 않고 한계가 있다. 따라서 CoQ_{10} 결핍성 사구체병증의 병태생리를 규명하고 최적의 치료 조건을 확립하는 것이 필요하다.

이 연구에서는 CoQ_{10}이 결핍된 세포 및 동물 모델(*Adck4*$^{\Delta Podocyte}$ 마우스)과 신장 오가노이드를 이용해 CoQ_{10} 결핍이 미치는 영향을 분석하였다. ADCK4 결실로 인한 CoQ_{10} 결핍은 미토콘드리아 기능 이상을 초래하였고, 특히 막전위($\Delta\Psi m$)의 감소가 확인되었다. 이러한 변화는 HK-2 세포에서는 관찰되지 않아, 족세포가 CoQ_{10} 결핍에 더 취약함을 시사한다. 또한, CoQ_{10} 결핍 족세포에서는 산화 스트레스가 증가하였다.

ADCK4는 COQ5와 직접 상호작용하며 COQ 복합체의 안정성 유지에 관여하고, ADCK4 결손 시 COQ 단백질 수준과 OXPHOS 복합체 III의 발현이 감소하는 양상이 확인되었다. CoQ_{10} 결핍 신장 오가노이드에서는 전체적인 구조는 유지되었으나, 족세포 내 미토콘드리아 이상이 관찰되어 CoQ_{10}이 신장 발달과 족세포 건강에 중요한 역할을 한다는 점을 보여준다.

CoQ_{10} 결핍 iPSC(*PDSS2, COQ2, ADCK4*-KO 유래)에서 유래한 신장 오가노이드를 단일세포 전사체 분석한 결과, 세포 구성에는 큰 변화가 없었으나, 족세포에서 특징적인 전사체 변화가 확인되었다. 산화적 인산화 경로의 하향 조절과 TGF-β 신호전달, 상피-간엽 전이, 세포사멸 경로의 상향 조절이 나타나, 미토콘드리아 기능 저하와 초기 손상 반응을 반영한다.

또한 마우스 모델을 이용하여 CoQ_{10} 전구체 유사체인 2,4-dihyroxybenzoic acid(2,4-diHB)와 치료 후보 약물인 Probucol와 Aspirin의 치료 효과를 시점에 따라 비교하였고 그 결과, 3개월 시점에서의 조기 투여는 신장 기능을 보존했지만, 5개월 이후의 지연 투여는 효과가 없었음을 밝혔다. 이는 병이 진행된 이후에는 치료 효과가 제한됨을

의미한다.

이 연구는 ADCK4가 CoQ_{10} 항상성과 족세포 유지에 필수적이라는 점을 강조하며, CoQ_{10} 결핍이 미토콘드리아 기능 이상과 진행성 사구체 손상을 유도한다는 것을 입증하였다. CoQ_{10} 결핍 신장 오가노이드는 질병 기전을 연구하고 타겟 치료제를 평가할 수 있는 유용한 플랫폼이 될 수 있다. 특히, 조기 투여의 중요성이 부각되며, CoQ_{10} 결핍성 신증의 임상 개입 시기를 설정하는 데 중요한 근거를 제공한다.

핵심되는 말 : 신증후군; 코엔자임 Q10; PDSS2; COQ2; COQ6; ADCK4; 원발성 코엔자임 Q_{10} 결핍; 신장 오가노이드; 단일세포 RNA 시퀀싱; 족세포